Jurnal Teknologi

Full Paper

THE EFFECT OF TRAVEL SPEED AND ELECTRICAL CURRENT ON PHYSICAL AND MECHANICAL PROPERTIES OF CNC MIG WELDED LOW CARBON STEEL PLATE A36

Agus Sifa[a]*, Leo Van Gunawan[b], Annifah[a], Badruzzaman[a]

[a]Department of Manufacture Design, Politeknik Negeri Indramayu, Indramayu, Jawa Barat, Indonesia

[b]Department of Mechanical Engineering, Politeknik Negeri Indramayu, Indramayu, Jawa Barat, Indonesia

Article history
Received
23 January 2024
Received in revised form
29 June 2024
Accepted
23 October 2024
Published Online
28 April 2025

*Corresponding author
agus.sifa@polindra.ac.id

Graphical abstract

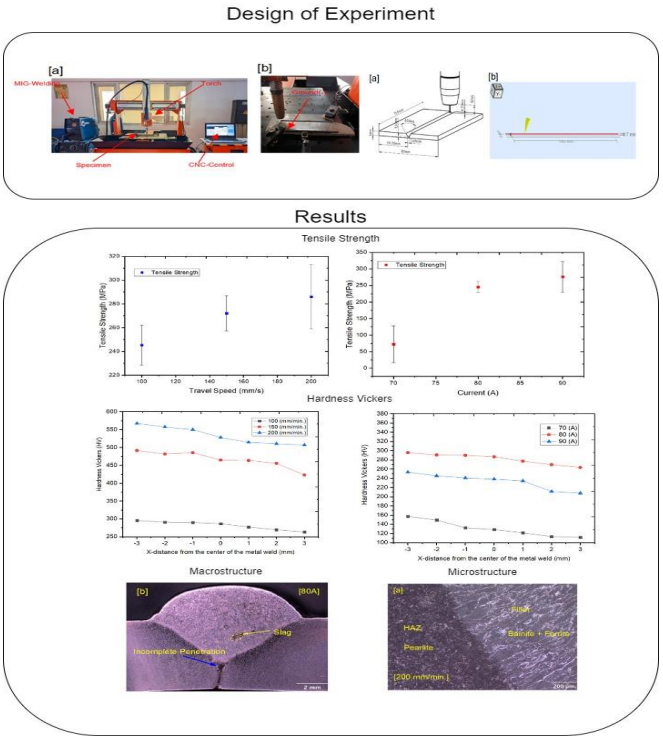

Abstract

The MIG welding process is widely used in industry because it is cost-effective, can be done with all positions, and has high productivity. The accuracy of the welding process and the relative welding parameters influence the welding quality. A CNC welding system can be used in welding to produce precise and stable welds. The experimental welding process in this study used materials ASTM A36, the welding process on a CNC MIG machine with current and travel speed parameters. The experimental results of the welding process identify defects with the Non-Destructive Test (NDT)-Liquid Penetrant Test (LPT)/Dye-Penetrant Test and Destructive Test (DT) including Tensile Test, Hardness Vickers, Macrostructure, and Microstructure, aimed at determining defects that occur. The results of the NDT and DT tests showed that there were porosity defects on the surface, slag, and incomplete penetration in the internal area of the metal weld. The welding results are best visually with a dye penetrant test at a current of 70 A a travel speed of 100 mm/min, and 80 A travel speed of 150mm/min and 200 mm/min. The hardness test results show that there is an influence on the welding current and travel speed. The tensile test results of welding results show the influence of current and travel speed, where the highest tensile strength at a current of 90A is 278 MPa, and the tensile strength at a travel speed of 200 mm/minute has a tensile strength of 286 MPa.

Keywords: CNC-MIG, defect, current, travel speed, low carbon steel

© 2025 Penerbit UTM Press. All rights reserved

1.0 INTRODUCTION

The metal inert gas (MIG) welding process is one of the gas metal arc welding (GMAW). In the MIG welding process, an inert shielding gas is used to pass through the nozzle and produce an electric arc, and all types of materials can be used in the MIG welding process. The MIG welding process is widely used in industry because it is cost-effective, with all positions, and has high productivity [1,2]. Some of the disadvantages of the MIG welding process include producing a lot of sparks, smoke, and an unstable arc [3]. Heat generated during the MIG welding process can change the microstructure and hardness of the

welding area [4]. Several parameters that influence the MIG welding process include current, voltage, gas flow rate, and the stickout between the nozzle and plate in the butt joint welding process [5].

Adin and İşcan (2022) have researched the influence of the current and position angle of MIG welding on medium carbon steel, that can affect tensile strength and elongation [6]. Abbasi *et al.* (2012) conducted experiments on the MIG welding process and analyzed the effect of welding speed, and heat rate on penetration, the characteristics, and the shape of the bead [7]. Furqan and Amarnadha (2020) studied the MIG welding process on mild steel materials regarding the effect of current, voltage, and speed on the tensile strength and hardness of the weld area [8]. Majeed *et al.* (2021) optimized welding parameters on the carbon steel using MIG welding by welding speed, current, and wire feed speed, which influence the tensile strength and hardness of the weld area [9]. Hooda *et al.* (2012) optimized the tensile strength of MIG welding on medium carbon steel plate materials, carried out longitudinal tensile tests with that strength results stronger than traversal tensile tests, and compared the microstructure tests [10]. Frih *et al.* (2015) identified the impact of MIG welding porosity on microstructure and hardness, where the welding area where porosity occurs has low hardness [11]. Fahad and Alkhafaji (2022) identified the influence of speed and current parameters on welding defects in low-carbon steel, which have identified visually the visible welding quality. The form of porosity, underfill and crack defects. Current and speed affect the hardness of the welding area [12].

Qays (2022) conducted research comparing the results of MIG welding with other welding, evaluating the mechanical properties of the welding results, where the results of MIG welding have the best mechanical properties compared to other processes, and the HAZ size is smaller [13]. Djuhana and Muljadi [2019] researched A36 material to determine the microstructure and mechanical properties using a current of 95-120 A at a current of 95 A, which has a hardness value close to the hardness value of the base material [14]. Kedir *et al*. (2022) analyzed the characteristics of butt joints MIG Welding with a plate thickness of 2 mm by testing macrostructure, microstructure, and mechanical properties, showing that welding parameters contributed to the characteristics of the welding results [15].

Several efforts can prevent defects in the result welding process and improve the welding process quality. A welding process's accuracy and relative welding parameters influence the quality of the welding results [16]. Salunke *et al.* (2020) carried out improvements and new welding techniques with an automation system to improve the quality of welds on pipes and shafts using constant parameters [17]. Dmello *et al.* (2017) designed and manufactured a 2-axis MIG welding process automation system for flat welding processes [18]. Ghazvinloo *et al.* (2010) have researched the influence of voltage, current, and welding speed parameters using a robotic MIG welding system and stated that a linear increase between current and voltage is influenced by penetration depth [19]. Sudhakar, *et al.* (2018) have researched automatic welding on ASTM A106 Grade B material and stated that welding with automatic settings can improve the quality of welding results, automatic welding results are defect-free, and welding results are consistent [20]. Mustafa and Rao (2016) stated that welding machine automation has many benefits, such as maintaining healthy workers and reducing errors and problems during the welding process using constant welding travel speed [21]. Frolov (2020) states that the cost-reduction welding process by building an automation system, can reduce welding failures [22]. The continuous movement of the welding process needs planning well [23], and a precise movement system can produce precise results in welding [24]. The Computer Numerical Control (CNC) welding system is a system that can be used in the welding process to produce precise and stable weld results [25]. The welding movement in the CNC system depends on the trajectory profile of the automatic system [26].

Based on problems during the welding process, especially with the A36 material, which is easy to find and widely used in industry [27], the effect of welding process parameters with a CNC welding system needs to be evaluated, especially regarding the travel speed and electrical current on physical welding to regarding welding defects. This research aims to evaluate the influence of looking for the best travel speed, current, and welding results, by evaluating external and internal defects through macrostructure, microstructure changes, and mechanical properties.

2.0 MATERIALS AND METHODOLOGY

2.1 Materials

The experimental process in this research uses ASTM A36 low-carbon steel material. ASTM A36 material with mechanical specifications and chemical composition in Table 1 and Table 2, and chemical composition of filler wire ER70S-6 in Table 3, with a wire diameter of 0.8 mm.

Table 1 Properties Mechanical ASTM A36[28]

Mechanical Properties	Tensile Strength (MPa)	Yield Strength (MPa)	Elongation (MPa)	Hardness, Brinell
Values	400-550	250	20.0%	119 - 159

Table 2 Chemical Composition (wt %) of A36 [27,28]

Element	C	P	Si	Mn	S	Fe	Cu
Composition (Max)	0.026	0.04	0.40	1.03	0.05	98.0	0.2

Table 3 Chemical Composition (wt%) of filler wire ER70S-6 [27]

Element	P	Si	Mn	S	Ni	C	Cr	Mo	V
Composition (Max)	0.018	0.828	1.543	0.05	0.014	0.082	0.033	0.15	0.3

2.2 Methodology

CNC - MIG Welding system has movement with the main components of the X, Y, and Z axis system, equipped with a CNC control system that is integrated with a MIG welding machine, as shown in Figure 1. CNC-MIG welding process using a Miller ST44 welding machine and pure gas CO_2 (99.99%). Figure 1 shows the automatic welding process with the CNC - MIG Welding.

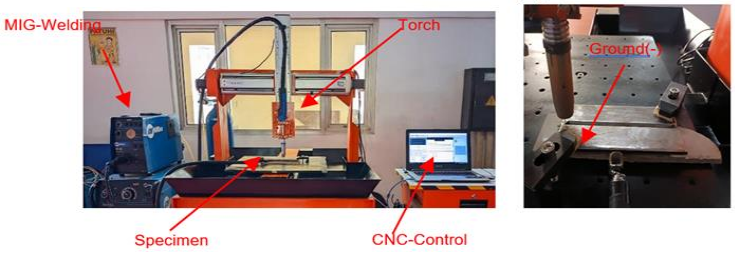

(a) (b)

Figure 1 Set-Up (a) CNC MIG welding, and (b)Specimen

Figure 2 shows the visual display of the UGS software for the automatic butt joint welding trial process using CNC-MIG. A G-Code was created so that it could be processed further to provide commands for the butt joint welding process.

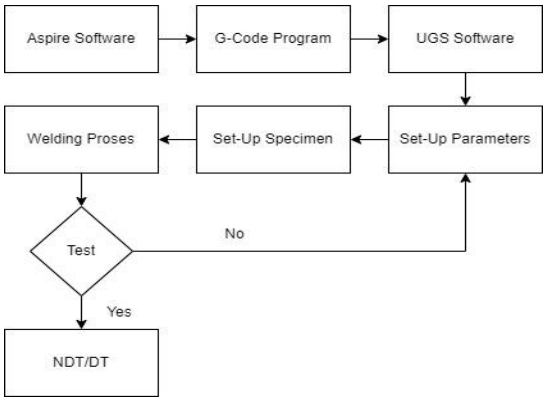

(a)

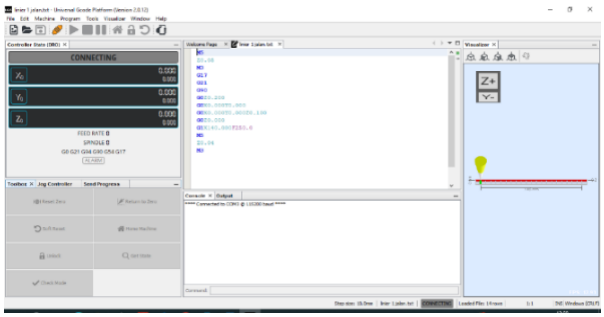

(b)

Figure 2 Set Up CNC Control (a) process procedures of CNC-MIG Welding, and (b) G-Code in the Software UGS

The welding process procedure with a CNC-MIG Welding machine is shown in Figure 2(a). Steps in the welding experimental process using a 3-axis CNC-MIG machine;

i. The first step is to create a toolpath for torch movement using Aspire Software. The movement toolpath that has been created is converted to a G-Code program for welding process movements.
ii. In the second step, the G-Code toolpath program is used in the UGS software (Figure 2(b)) to control the torch movement program on the CNC-MIG Welding machine with hardware control to control the torch travel speed, control the on/off of the wire feeder and the CO_2 gas shield.
iii. The third step is to set the welding parameters, setting the gas pressure and height of the contact tip work distance to the specimen on the CNC MIG welding machine.
iv. The fourth step is setting the input current parameters.
v. The fifth step is conducting CNC MIG welding experiments.

The dimensions of the welding experimental specimens refer to ISO 9692-1:2013(E) [29,30], as in Figure 3.

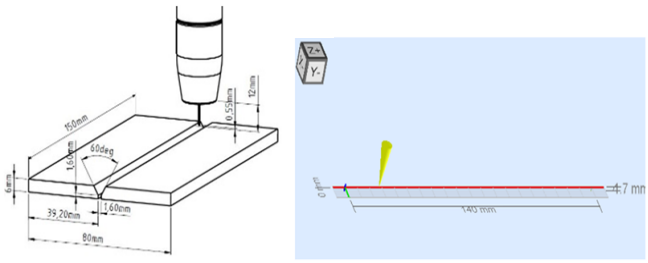

(a) (b)

Figure 3 Design of experiment welding process (ISO 9692-1:2013(E)), (a) Dimension of the specimen and, (b) toolpath welding process

Figure 3(a) dimensions of the experimental specimen, where the plate length is 150 mm with a width of 39.2 and a total width of 80 mm, with the but joint welding position, where the penetration depth is 1.6 mm, and the bevel angle is 60°, the plate thickness is 6 mm and the distance 0.55 mm tip wire contact. Figure 3(b) illustrates the toolpath in UGS software with a torch movement length of 140 mm.

The welding process results were evaluated using The Non-Destructive Test (NDT)-dye penetrant and Destructive Test (DT). DT includes tensile tests, hardness tests, macrostructure, and microstructure tests.

After carrying out NDT testing on the welding results, sample preparation is then carried out for testing hardness, macrostructure, and microstructure. Macrostructure, microstructure, and hardness test samples were made by cutting the welding results in the middle part that was free of defects. Tensile test preparation is carried out by making different samples

and continuously welding using dimensions according to ISO 6892-1:2009 [31].

The etching process for macrostructure and microstructure test specimens is immersed in HNO_3 and 96% alcohol for 5 seconds.

The tensile test process of the welding results is shown in Figure 4. The dimensions of the tensile test object are shown in Figure 5 and the shape of the plate model. Referring to the test standard: ISO 6892-1:2009 [31].

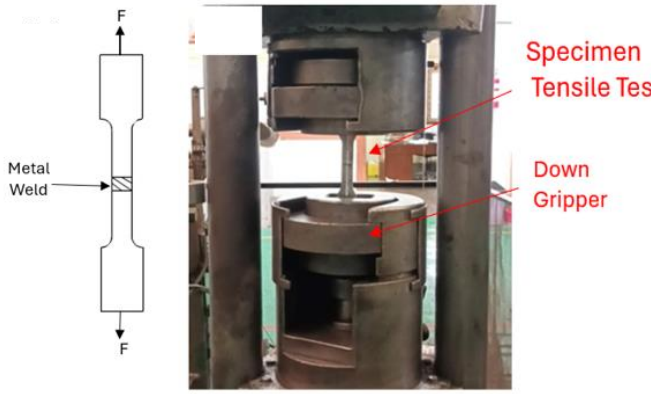

(a) (b)

Figure 4 Set up of tensile test, [a] fracture mode, [b] tensile test process

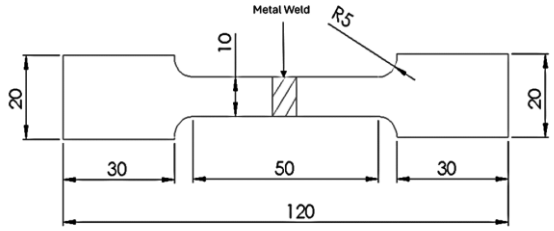

Figure 5 Dimension of tensile test specimen [5]

The hardness test process uses the Innova Verzus 700AS type test machine. Figure 6(a) Vickers hardness testing process, where the hardness test specimen made from welding results, the specimen resulting from the welding experiment is cut in the middle as shown in Figure 6(b) to carry out the hardness test, the hardness test taken in the metal weld area with the amount 7 points as in Figure 6(c), where the distance between the hardness test points is ± 1 mm.

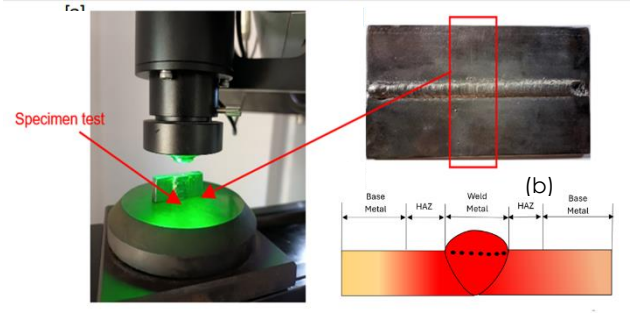

(a) (c)

Figure 6 Hardness Vickers test, [a] Hardness test process, [b] hardness specimen test,[c] point of hardness test

The results of welding experiments carried out macrostructure testing to determine internal defects in the welding area using an Olympus GX71 digital microscope are shown in Figure 7.

Figure 7 Digital microscope Olympus GX71

The etching process for microstructure and macrostructure test samples is carried out by immersion for approximately 5 seconds in a solution of HNO_3 and 96% alcohol. Measurement of the size of weld defects using imageJ software, distance in a figure with a pixel aspect ratio of 1 has a value of 407.5028 pixels: 2 mm.

3.0 RESULTS AND DISCUSSION

3.1 Non-Destructive Test

The MIG welding process results evaluated defects with a non-destructive test (NDT) using a dye penetrant test/liquid penetrant testing (LPT). NDT aims to visually identify external defects from the welding process result [32].

Figure 8 shows the results of welding experiments and dye penetrant tests with travel speed variations of 100mm/min, 150mm/min, and 200 mm/min and a constant current of 80A, where the results of experiments with input variations in travel speed and current. The results of the dye penetrant test show defects visually on the surface [33] with a red indicator. Figure 8(a) There are welding defects in the form of underfill at the start point and endpoint positions. Figure 8(b) shows welding defects in the shape of craters at the start point, endpoint, and porosity positions in the middle area of the surface. Figure 8(c) shows welding defects are underfilled at the start point, and endpoint, porosity, and incomplete fusion. The torch movement process is too fast in the middle area and has more porosity defects compared to the welding results with a travel speed of 150 mm/min and 100 mm/min. The results of the dye penetrant test on travel speed variations have better welding results visually, and fewer defects occur at an input travel speed of 100 mm/min.

The results of welding process experiments and dye penetrant tests with current parameters of 70 A, 80A, and 90A, and constant travel speed (100 mm/min), can be seen in Figure 8(d) are shown underfill defects at the start point and end-point positions and incomplete fusion in the middle area, Figure 8(e) and Figure 8(f) show welding defects that occur only in the underfill at the start point and end-point positions, so based on the results of the visual dye penetrant test and the defects that occur, the best welding results are at a current of 80A and 90A and a travel speed of 100 mm/min.

Figure 8 Results of welding and dye penetrant test, current parameters; (a) 70A,100 mm/min, (b) 80A,100 mm/min, (c) 90A,100 mm/min; Travel Speed Variation;(d) 80A,100 mm/min, (e) 80A,150 mm/min, and (d) 80A,200 mm/min

Table 4 shows the criteria for defects that occur as a result of the LPT, visually referring to ASTM E165 [34] grouped as indications of defects in the rejected criteria for all specimens occurring at the endpoint due to accumulation during the welding process, the accepted criteria at the start point on specimens a, d and e, for indications of defects in the middle position occurring in specimens a, e and f.

Table 4 Criteria Indication of defects

Specimens	Size of discontinuity (mm)	Position	Indication	Remark
a	1	Start point	Underfill	Accepted
	-	Middle	Not defects	Accepted
	13	Endpoint	Underfill	Rejected
b	8	Start point	Creater	Rejected
	6	Middle	Porosity	Rejected
	9	Endpoint	Creater	Rejected
c	4	Start point	Underfill	Rejected
	3	Middle	Porosity	Accepted
	8	Middle	Incomplete Fusion	Rejected
	9	Endpoint	Underfill	Rejected
d	2	Start point	Underfill	Accepted
	6	Middle	Incomplete fusion	Rejected
	10	Endpoint	Underfill	Rejected
e	2	Start point	Underfill	Accepted
	-	Middle	Not defects	Accepted
	12	Endpoint	Underfill	Rejected
f	4	Start point	Underfill	Rejected
	-	Middle	Not defects	Accepted
	7	Endpoint	Underfill	Rejected

3.2 Destructive Test

a. Tensile Test

The specimen tensile test results are shown in Figure 9.

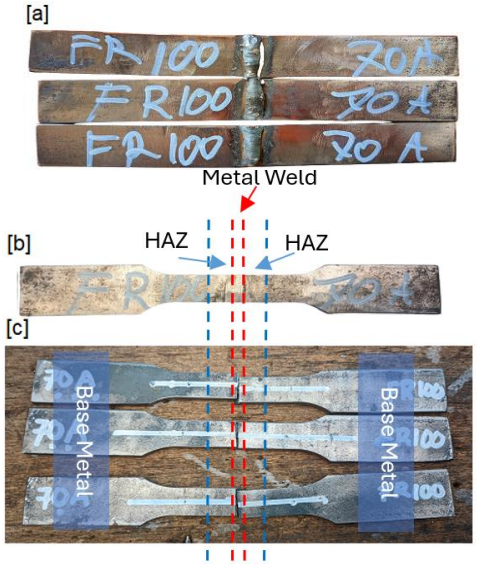

Figure 9 Test Specimens(a) Welding Results, (b) Preparation Tensile test, (c) Test specimen results from tensile test

Tensile tests were carried out on three specimens for each parameter. Tensile testing of the welding process results with current parameters of 70 A, 80 A, and 90 A and a constant travel speed of 100 mm/minute. Tensile tests were done with three tests on each variable current parameter. The tensile test results are shown in Figure 10.

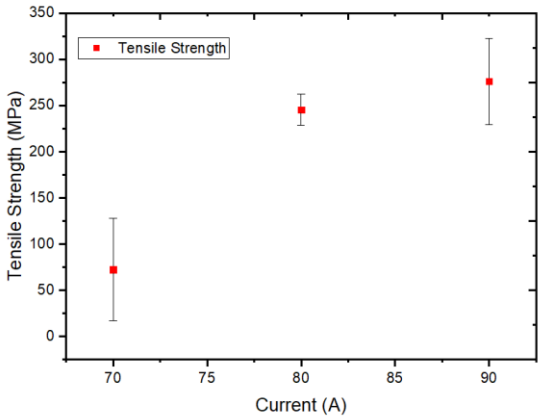

Figure 10 Tensile test results-current variations

Figure 10 shows the tensile test results of current parameters. The welding results with a current of 70 A show an average tensile strength value of 72.3 MPa with a standard deviation of 51.84. The welding process results in a current of 80 A showing a value of 245.3 MPa with a standard deviation of 16.77. The welding process results in a current of 90 A and has a tensile strength of 278 MPa with a standard deviation of 46.35. Tensile test results on welding results with varying currents show that the tensile strength of the welding results is below the tensile strength value of the A36 base material (Table 1), and the condition of a metal weld is fractured in the weld area. Figure 10 shows the influence of current on welding results [35]. The greater the current given during welding, the greater the tensile strength value, and current contributes greatly to tensile strength [36].

Figure 11 shows the tensile test results on welding results with travel speed variations of 100 mm/minute, 150 mm/minute, and 200 mm/minute with a current of 80 A. The Tensile test results at a travel speed of 100 mm/minute have an average tensile strength of 245.3 MPa with a standard deviation of 16.77. Travel Speed of 150 mm/minute has an average tensile strength of 272 MPa with a standard deviation of 14.79, and travel speed of 200 mm/minute has an average tensile strength of 286 MPa with a standard deviation of 27.08.

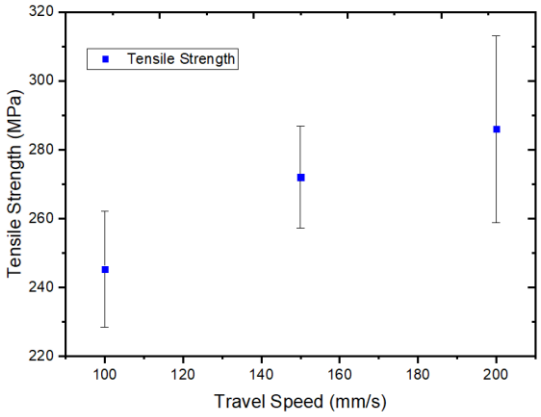

Figure 11 Tensile test results of travel speed variations

Table 5 presents the fracture mode of tensile test results, with overall results of fractures occurring in metal welds in brittle mode.

Table 5 The fracture mode of tensile test results

Specimens	Location	Av. Tensile Strength (MPa)	Fracture Mode
a	Metal Weld	72.3	Brittle
b	Metal Weld	245.3	Brittle
c	Metal Weld	278	Brittle
d	Metal Weld	245.3	Brittle
e	Metal Weld	272	Brittle
f	Metal Weld	286	Brittle

b. Hardness Vickers

The Vickers method's hardness test uses a load of 20 kgf and an indentation time of 15 seconds. The hardness test method according to ASTM E-384 specifies a diamond indenter with an angle between facing surfaces of 136° [37]. In this study, hardness testing (Vickers) was carried out to know the distribution of hardness in the area of the metal weld.

The welding process results are made for hardness specimens tested in the welding area. The hardness test is carried out on the metal weld as shown in Figure 6, where the hardness test of welding process results with current parameters are presented in Figure 12, and the hardness test of the welding process results with travel speeds are shown in Figure 13.

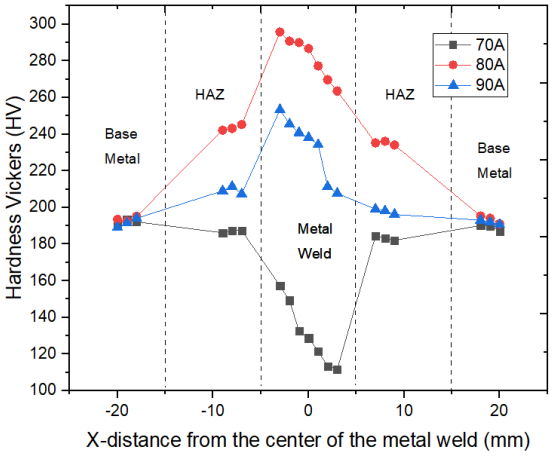

Figure 12 Hardness Vickers test results (current)

Figure 12 presents the results of hardness test data processing (Vickers) in the metal weld area, Heat Affected Zone (HAZ), and Base Metal. The hardness test results with a current of 70 A in the metal weld area have an average hardness test result value of 130.6 HV. The hardness test results with a current of 80 A in the metal weld area have an average hardness test result of 282 HV, and the hardness test results with a current of 90 A in the metal weld area have an average hardness test result of 233 HV. The welding results with a current of 90 A in the metal weld area have lower hardness test results than currents of 70 A and 80 A. The 90 A current has an increase in heat so increasing the current reduces hardness [12].

Figure 13 shows the results of the hardness test in the weld metal area, HAZ, and base metal using the movement speed parameter. Hardness test data processing (Vickers) with an input movement speed of 100 (mm/minute) in the metal welding area has an average hardness test result value of 282 HV. At an input travel speed of 150 (mm/minute), the hardness test results in the metal weld area averaged 465.6 HV. At an input travel speed of 200 (mm/minute), the hardness test results obtained in the metal weld area were an average of 533.5 HV. The hardness test results

on the welding process result with travel speed parameters show that the greater the travel speed input value, the smaller the hardness value obtained, and the hardness of the welding results is greater than the material A36 [38] has 190 HV [39].

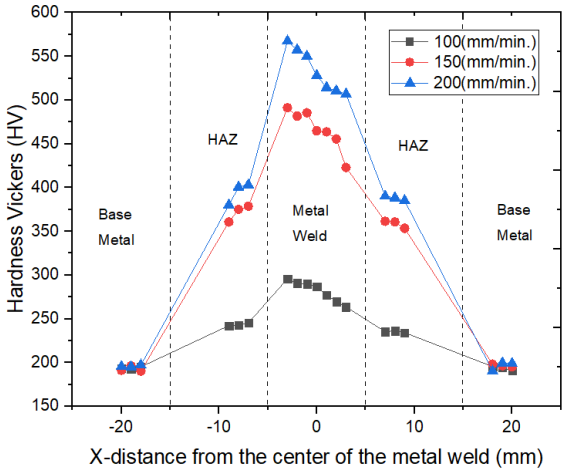

Figure 13 Hardness Vickers test results (travel speed)

Table 6 presents a comparison of the results of the hardness test and tensile test due to current and travel speed. The increase in the travel speed that occurs affects the hardness test and increases the results of the tensile strength test [40].

Table 6 Hardness Test Results Vs Tensile Strength Results

Current (A)	Travel Speed (mm/min.)	Av. Hardness Vickers (HV)	Av. Tensile Strength (MPa)
70	100	130.6	72.3
80	100	282	245.3
90	100	233	278
80	100	282	245.3
80	150	466.6	272
80	200	533.5	286

c. Macrostructure

Macrostructure testing is carried out to determine internal defects in the welding results. Figure 13 shows the results of metallography tests on experimental results with current variations of 70A, 80A, and 90 A with a travel speed of 100 mm/minute. The results of the metallography test with 12x magnification are shown in Figure 14(a) with a current of 70 A. The metallography results show that internal defects in the welding results are slag on the bottom (yellow arrow direction) an area of 0,28 mm^2 and porosity on the top surface (red arrow direction) due to oxygen and nitrogen that is trapped [32], Figure 14(b) results of welding with a current of 80A show slag defects (red arrow direction) has area of 0.25 mm^2 and incomplete penetration occurs (yellow arrow direction), Figure 14(c) results of welding with a current of 90A show incomplete penetration defects (yellow arrow direction) a 0.33 mm^2. The welding results with a current of 70 show better welding results

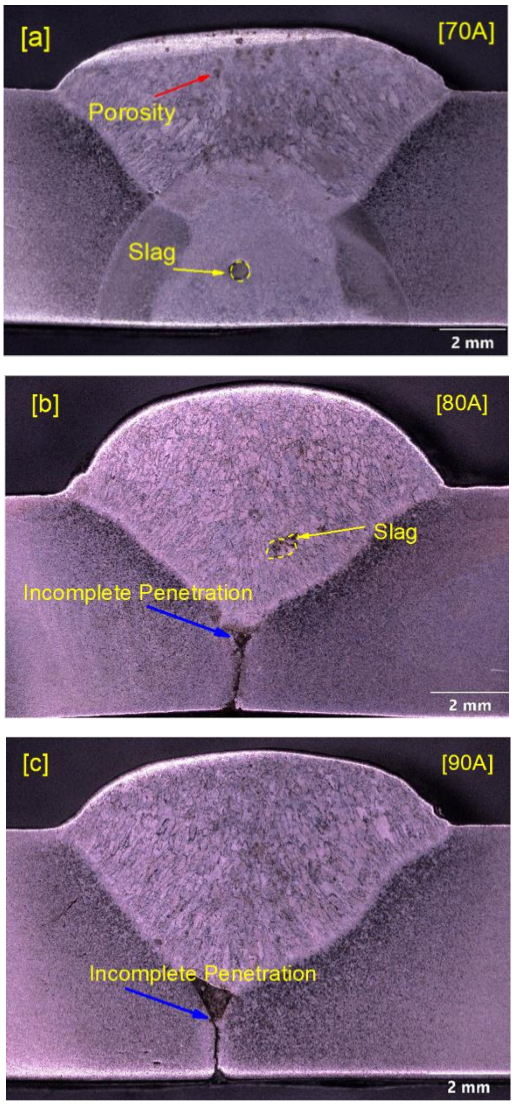

Figure 14 Macrostructure test of welding process with current parameters, (a) 70A, (b) 80A, and (c) 90A

Figure 15(a) shows the results of metallography testing on metal welds at a travel speed of 100 mm/minute, which shows slag defects (blue arrow direction) have an area of 0.24 mm^2 and incomplete penetration (yellow arrow direction). Figure 15(b) shows the welding results using a travel speed of 150 mm/minute. There are porosity defects on the surface (blue arrow direction) and incomplete penetration (yellow arrow direction). Figure 15(c) shows the metallography results of welding at 200 mm/minute. There are porosity defects on the surface (blue arrow direction), slag defects (direction blue arrow) has an area of 0.24 mm^2, incomplete penetration (blue arrow direction), and travel speed parameters, which have incomplete penetration at a travel speed of 100 m/s.

Incomplete penetration defects are caused by the influence of travel speed and angle or position of welding [41].

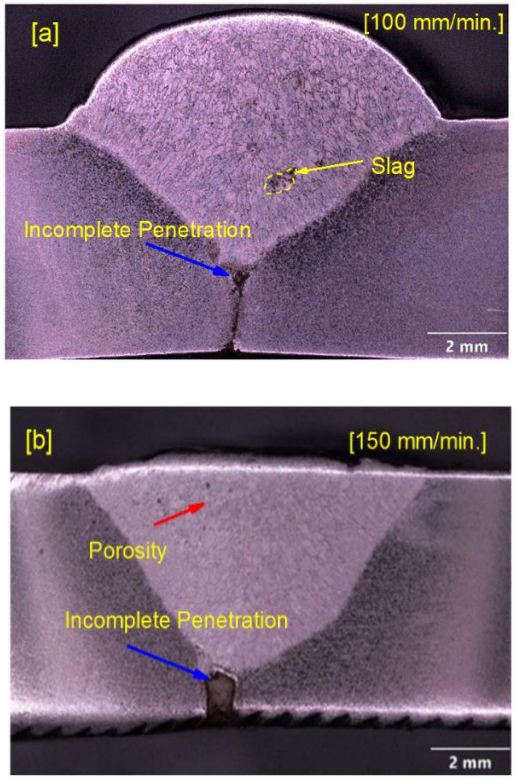

Figure 15 Macrostructure test of welding process with travel speed parameters, (a)100 mm/minute, (b)150 mm/minute, and (c) 200 mm/minute

c. Microstructure

Microstructure testing is carried out on welding results to determine the effect of current and travel speed on the welding microstructure, especially in the Heat Affected Zone (HAZ) and filler area. Microstructure testing is carried out on welding results to determine the effect of current and travel speed on the welding microstructure, especially in the HAZ and filler area.

Figure 16 shows the results of microstructure metallography with travel speed variations of 200mm/minute, 150mm/minute, and 100 mm/minute with a current of 80A. Figure 16(a) and Figure 16(b) show the results of welding with a travel speed of 200 mm/minute and a travel speed of 150 mm/minute in the HAZ showing pearlite (black), and the filler area is bainite and ferrite (white) [42], Figure 16(c) results of welding with a travel speed of 100 mm/minute shows that the HAZ is pearlite and ferrite, and the filler area is bainite and ferrite.

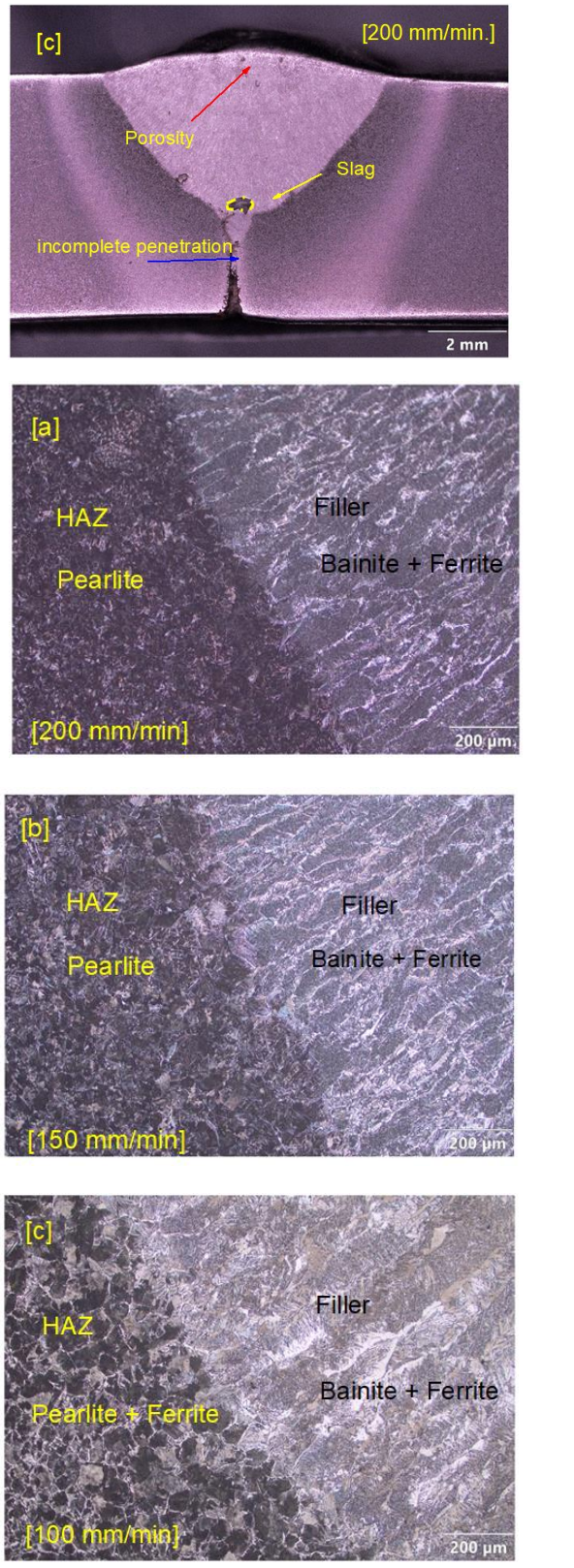

Figure 16 Microstructure, (a) 200 mm/minute, (b)150 mm/minute, and (c) 100 mm/minute

Figure 17 shows the welding results with current parameters of 90A, 80 A, and 70A with a travel speed of 100 mm/minute with a microstructure in the HAZ in the form of pearlite and ferrite. The filler area shows the grains bainite and ferrite. The current parameters do not significantly affect the microstructure of the welding process resulting show a consistent and stable welding process.

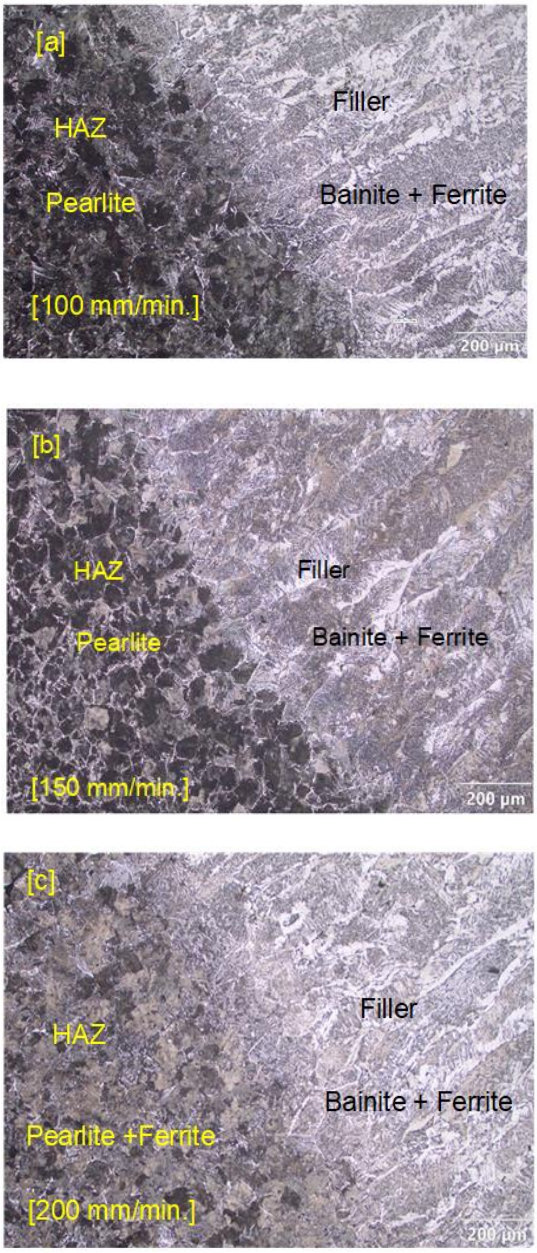

Figure 17 Microstructure (a) 90A,(b) 80A, and (c)70A

4.0 CONCLUSION

In this study, the results of welding experiments with variations in travel speed and current using a CNC MIG welding machine can be concluded that the welding results are best visually with a dye penetrant test at a current of 70A and a travel speed of 100 mm/min, and 80 A travel speed of 150mm/min and 200 mm/min. The hardness test results show that there is an influence on the welding current and travel speed, where the hardness value is large at a current of 90A and a travel speed of 100 mm/min, and 80 A at a travel speed of 200 mm/min. The macrostructure test results show several defects in each welding result in the form of porosity, slag, and imperfect penetration defects. Microstructure test results in the HAZ in the form of pearlite and ferrite. The filler area shows the grains of bainite and ferrite. The current parameters do not significantly affect the microstructure of the welding process resulting in a consistent and stable welding process. In the variation of travel speed, the results of welding with on travel speed of 100 mm/minute show that the HAZ is pearlite and ferrite, and the filler area is bainite and ferrite, which is different from the microstructure results at 150 mm/min and 200 mm/min containing pearlite grains. HAZ contains bainite and ferrite grains in the filler area. The tensile test results of welding results show the influence of current and travel speed, where the highest tensile strength at a current of 90A is 278 MPa, and the tensile strength at a travel speed of 200 mm/minute has a tensile strength of 286 MPa.

Acknowledgment

This research is fully supported by the Center for Research and Community Service- Politeknik Negeri Indramayu grant, 0856/PL42.11/AL.04/2023. The authors fully acknowledged the Center for Research and Community Service and Department of Engineering -Politeknik Negeri Indramayu.

Conflicts of Interest

The author(s) declare(s) that there is no conflict of interest regarding the publication of this paper.

References

[1] Bera, T. 2020. The History of Development of Gas Metal Arc Welding Process. *Indian Science Cruiser*. 34(4): 64–66. Doi:https://doi.org/10.24906/isc%2F2020%2Fv34%2Fi6%2F208225.

[2] Ogbonna, O. S., Akinlabi, S. A., Madushele, N., Mashinini, P. M., and Abioye, A. A. 2019. Application of MIG and TIG Welding in Automobile Industry. *Journal of Physics: Conference Series*. 1378(4): 042065. Doi: https://doi.org/10.1088/1742-6596/1378/4/042065.

[3] Ogundimu, E. O., Akinlabi, E. T., and Erinosho, M. F. 2019. Comparative Study between TIG and MIG Welding Processes. *Journal of Physics: Conference Series*. 1378(2): 022074. Doi: https://doi.org/10.1088/1742-6596/1378/2/022074.

[4] Mahdi, E., Eltai, E. O., and Rauf, A. 2014. The Impact of Metal Inert Gas Welding on the Corrosion and Mechanical Behavior of AA 6061 T6. *International Journal of Electrochemical Science*. 9(3): 1087–1101.

Doi: https://doi.org/10.1016/S1452-3981(23)07780-5.
[5] Ghosh, N., Pal, P. K., and Nandi, G. 2016. Parametric Optimization of MIG Welding on 316L Austenitic Stainless Steel by Grey-based Taguchi Method. *Procedia Technology*. 25: 1038–1048. Doi: https://doi.org/10.1016/j.protcy.2016.08.204.
[6] Adin, M. Ş., and İşcan, B. 2022. Optimization of Process Parameters of Medium Carbon Steel Joints Joined by MIG Welding using Taguchi Method. *European Mechanical Science*. 6(1): 17–26. Doi: https://doi.org/10.26701/ems.989945.
[7] Abbasi, K., Alam, S., and Khan, M. I. 2012. An Experimental Study on the Effect of MIG Welding Parameters on the Weld-bead Shape Characteristics. *Engineering Science and Technology: An International Journal (ESTIJ)*. 2(4): 599–602.
[8] Furqan, A., and Amarnadha, M. 2020. Optimization of Mig Welding Parameters for Improving Strength of Welded Joint. *Journal of Interdisciplinary Cycle Research*. 6: 128–135. Doi:18.0002.JICR.2020.V12I8.008301.31712157.
[9] Majeed, N. H., Radhi, H. E., & Abid, H. J. 2021. Optimization of MIG Welding Parameters. *University of Thi-Qar Journal for Engineering Sciences*. 11(2): 1–7. Doi: http://www.doi.org/10.31663/tqujes.11.2.382(2021).
[10] Hooda, A., Dhingra, A., and Sharma, S. 2012. Optimization of MIG Welding Process Parameters to Predict Maximum Yield Strength in AISI 1040. *International Journal of Mechanical Engineering and Robotics Research*. 1(3): 203–213.
[11] Frih, I., Adragna, P. A., and Montay, G. 2015. Influence of a Welding Defect on a HSLA S500MC Steel Plate: Microstructure and Residual Stress Evaluation. *Proceedings of the 6th International Conference on Mechanics and Materials in Design*. 169–180.
[12] Fahad, N. D., and Alkhafaji, M. M. A. 2022. Investigation of MIG Welding Process Parameters on Welding Defects and Hardness of Low Carbon Steel Weld Joints. *International Journal of Energy and Environment*. 13(3): 113–120.
[13] Ismael, Q. H. 2022. Investigation of Mechanical Properties of Low Carbon Steel Weldments for Different Welding Processes. *SVU-International Journal of Engineering Sciences and Applications*. 3(2): 116–122. Doi: 10.21608/SVUSRC.2022.152920.1061.
[14] Djuhana, M. 2019. Influence of Variation of Electrical Current Welding of ASTM Steel A 36 on Microstructure and Mechanical Properties. *J. Phys. Conf. Ser*. 1204: 012014. Doi: http://doi.org/10.1088/1742-6596/1204/1/012014.
[15] Behredin, K. B., Janaki Ramulu, P., Habtamu, B., Besufekad, N., and Tesfaye, N. 2022. Characterization and Parametric Optimization of EN-10149-2 Steel Welded Joints Made by MIG Welding. *Advances in Materials Science and Engineering*. 2022. Doi: https://doi.org/10.1155/2022/8276496.
[16] Mahore, N., Sharma, T., and Singh, R. 2017. Study of MIG welding Process with Different Type Technique: A Review. *IJSTE-International J. Sci. Technol. Eng.* 4(6): 1–5.
[17] Salunke, S., Mali, M., Yande, O., and Kulkarni, V. 2020. Automatic Welding Machine for Exhaust Pipes Using MIG Welding Process. *International Research Journal of Engineering and Technology (IRJET)*. 7(6): 5791–5794.
[18] Dmello, S. S., Biju, J., Hegde, S. S., and Ganoo, A. V. 2017. Design and Fabrication of Automated 2-Axis Welding Machine. *International Journal of Mechanical Engineering and Technology*. 8(3).
[19] Ghazvinloo, H. R., Honarbakhsh-Raouf, A., and Shadfar, N. 2010. Effect of Arc Voltage, Welding Current and Welding Speed on Fatigue Life, Impact Energy and Bead Penetration of AA6061 Joints Produced by Robotic MIG Welding. *Indian Journal of Science and Technology*. 3(2): 156–162. Doi:10.17485/ijst/2010/v3i2.8.
[20] Sudhakar, R., Sivasubramanian, R., and Yoganandh, J. 2018. Effect of Automated MIG Welding Process Parameters on ASTM A 106 Grade B Pipe Weldments used in High-temperature Applications. *Materials and Manufacturing Processes*. 33(7): 749–758. Doi: https://doi.org/10.1080/10426914.2017.1401719.
[21] Mustafa, F. F., and Rao, M. I. 2016. Automatic Welding Machine for Pipeline using MIG Welding Process. *International Research of Engineering and Technology (IRJET)*. 3(12): 1–7.
[22] Frolov, A. V. 2021. Pipe Welding Machine Modernization. *Journal of Physics: Conference Series*. 2096(1): 012016. Doi: https://doi.org/10.1088/1742-6596/2096/1/012016.
[23] Liu, X., Qiu, C., Zeng, Q., and Li, A. 2019. Kinematics Analysis and Trajectory Planning of Collaborative Welding Robot with Multiple Manipulators. *Procedia Cirp*. 81: 1034–1039. Doi: https://doi.org/10.1016/j.procir.2019.03.247.
[24] Ali, S., Agrawal, A. P., Ahamad, N., Singh, T., and Wahid, A. 2022. Robotic MIG Welding Process Parameter Optimization of Steel EN24T. *Materials Today: Proceedings*. 62: 239–244. Doi: https://doi.org/10.1016/j.matpr.2022.03.091.
[25] Lin, H. 2011. Design of Special Welding Machine based on Open CNC System. *Communication Systems and Information Technology: Selected Papers from the 2011 International Conference on Electric and Electronics (EEIC 2011) in Nanchang, China on June 20-22, 2011*. 4: 839–844. Springer Berlin Heidelberg. Doi: https://doi.org/10.1007/978-3-642-21762-3_110.
[26] Verma, K., Belokar, R. M., Verma, V. K., and Ntalianis, K. 2019. Track-based Analysis for Profile Generation on Globoidal Cam in Automatic Tool Changer of CNC Machining Center. *Assembly Automation*. 39(2): 369–379. Doi: https://doi.org/10.1108/AA-08-2018-111.
[27] Baskoro, A. S., Hidayat, R., Widyianto, A., Amat, M. A., and Putra, D. U. 2020. Optimization of Gas Metal Arc Welding (GMAW) Parameters for Minimum Distortion of T Welded Joints of A36 Mild Steel by Taguchi Method. *Materials Science Forum*. 1000: 356–363. Trans Tech Publications Ltd. DOI:https://doi.org/10.4028/www.scientific.net/MSF.1000.356.
[28] AL-Musawi, M. A., and Ali, A. R. K. A. 2018. Fatigue Analysis of Welding Joints of ASTM A36 Low Carbon Steel by Using Finite Element Method. *Journal of University of Babylon for Engineering Sciences*. 26(4): 237–248.
[29] International Standard Organization (ISO). 2013. EN ISO 9692-1: 2013 Welding and Allied Processes—Types of Joint Preparation—Part. 1: Manual Metal. Arc Welding, Gas.-Shielded Metal. Arc Welding, Gas. Welding, TIG Welding and Beam Welding of Steels.
[30] Ferdinandov, N., Gospodinov, D., Ilieva, M., and Radev, R. 2021. Effect of the Root Gap on the Structure and Properties of High Strength Steel S700MC Welds. *Key Engineering Materials*. 890: 201–208. DOI:https://doi.org/10.4028/www.scientific.net/KEM.890.201.
[31] International Standard Organization (ISO). 2009. EN ISO 6892-1:2009, Metallic Materials –Tensile Testing –Part 1: Method of Test at Room Temperature.
[32] Deepak, J. R., Raja, V. B., Srikanth, D., Surendran, H., and Nickolas, M. M. 2021. Non-destructive Testing (NDT) Techniques for Low Carbon Steel Welded Joints: A Review and Experimental Study. *Materials Today: Proceedings*. 44: 3732–3737. Doi: https://doi.org/10.1016/j.atpr.2020.11.578.
[33] Reddy, K. A. 2017. Non-destructive Testing, Evaluation of Stainless Steel Materials. *Materials Today: Proceedings*. 4(8): 7302–7312. Doi: https://doi.org/10.1016/j.matpr.2017.07.060.
[34] Khalid, N., Zamanhuri, P. Z. N. M., and Baharin, F. A. S. 2017. A Study of Weld Defects of Gas Metal Arc Welding with Different Shielding Gasses. *ARPN Journal of Engineering and Applied Sciences*. 12: 2006–2011.
[35] Mahesh, S., and Appalaraju, V. 2017. Optimization of MIG Welding Parameters for Improving Strength of Welded

Joints. *International Journal of Innovative Technology and Research*. 5(3): 6453–6458.
[36] Shinde, A. P., Deshpande, A. R., Chinchanikar, S. S., and Kulkarni, A. P. 2017. Evaluation of Tensile Strength of a Butt-welded Joint Considering the Effect of Welding Parameters using Response Surface Methodology. *Materials Today: Proceedings*. 4(8): 7219–7227. Doi: https://doi.org/10.1016/j.matpr.2017.07.049.
[37] Endramawan, T., and Sifa, A. 2018. Non Destructive Test Dye Penetrant and Ultrasonic on Welding SMAW Butt Joint with Acceptance Criteria ASME Standard. *IOP Conference Series: Materials Science and Engineering*. 306(1): 012122. DOI: https://doi.org/10.1088/1757-899X/306/1/012122.
[38] Sivakumar, S., and Kumar, J. V. 2015. Experimental Investigation on MIG Welded Mild Steel. *International Journal of Machine and Construction Engineering*. 2(1): 2394–3025.
[39] Senthilkumar, S., Manivannan, S., Venkatesh, R., and Karthikeyan, M. 2023. Influence of Heat Input on the Mechanical Characteristics, Corrosion and Microstructure of ASTM A36 Steel Welded by GTAW Technique. *Heliyon*. 9(9). Doi: https://doi.org/10.1016/j.heliyon.2023.e19708.
[40] Saleh Elfallah, S. S. 2023. Study the Influence of Welding Parameters by Taguchi's Design on the Mechanical Properties of Welded Mild Steel (S235jr). *Jurnal Teknologi*. 85(4): 55–66. Doi:https://Doi.Org/10.11113/Jurnalteknologi.V85.19653
[41] Mandal, N. R. 2017. Welding Defects. In: Ship Construction and Welding. Springer Series on Naval Architecture, Marine Engineering, Shipbuilding and Shipping. 2. Springer, Singapore. Doi: https://doi.org/10.1007/978-981-10-2955-4_19.
[42] Khan, N. U., Rajput, S. K., Gupta, V., Verma, V., and Soota, T. 2019. To Study Mechanical Properties and Microstructures of MIG Welded High Strength Low Alloy Steel. *Materials Today: Proceedings*. 18: 2550–2555. Doi: https://doi.org/10.1016/j.matpr.2019.07.112.